HHS Public Access

Author manuscript

Biomacromolecules. Author manuscript; available in PMC 2022 April 14.

Published in final edited form as:

Biomacromolecules. 2019 September 09; 20(9): 3352–3365. doi:10.1021/acs.biomac.9b00133.

Injectable Catalyst-Free Poly (Propylene Fumarate) System Crosslinked by Strain Promoted Alkyne-Azide Cycloaddition (SPAAC) Click Chemistry for Spine Defect Filling

Xifeng Liu[a,b], **A. Lee Miller II**[b], **Hao Xu**[a], **Brian E. Waletzki**[b], **Lichun Lu**[*,a,b]

[a]Department of Physiology and Biomedical Engineering, Mayo Clinic, Rochester, MN 55905, USA

[b]Department of Orthopedic Surgery, Mayo Clinic, Rochester, MN 55905, USA.

Abstract

A new PPF-BCN/hyPCL32-N_3 injectable system that can be crosslinked by catalyst-free, strain promoted alkyne-azide cycloaddition (SPAAC) click chemistry was developed for tissue engineering applications. The system was consisted of two components: PPF-BCN, poly (propylene fumarate) (PPF) functionalized with (1R,8S,9s)-bicyclo[6.1.0]non-4-yn-9-ylmethanol (BCN-OH), and hyPCL32-N_3, a hyper-branched 32-arm poly(ε-caprolactone) (PCL) dendrimer functionalized with azide as the cross-linker core. Fast SPAAC click reaction allowed the desired gelation of the system without using any toxic initiator or catalyst. Compared to the conventional injectable formulation, e.g., poly(methyl methacrylate)(PMMA), our PPF-BCN/hyPCL32-N_3 (abbreviated as PFCL-Click) injectable system showed enhanced biocompatibility and low heat generation during crosslinking. After reaction, the crosslinked PFCL-Click scaffolds supported excellent proliferation and differentiation of pre-osteoblast cells on the surface. The PFCL-Click system can be successfully injected into vertebral bodies of rabbit spine and can be monitored by X-ray imaging after incorporating zirconium dioxide (ZrO_2) powder. With these unique advantages, this injectable system has promising potential for bone defect repair and other tissue engineering and regenerative medicine applications.

Keywords

Tissue Engineering; Injectable; Biodegradable Polymer; Strain Promoted Alkyne-Azide Cycloaddition; Click Chemistry

[*]**Corresponding Author**: Lu.Lichun@mayo.edu. Tel.: 507-284-2267. Fax: 507-284-5075.

Author Contributions

The manuscript was written through the contributions of all authors. All authors approved the final version of the manuscript.

Supporting Information

NMR spectra of synthesized compounds, fluorescence images, and X-ray images (PDF). The Supporting Information is available free of charge on the ACS Publications website.

The authors declare no competing financial interest.

1. INTRODUCTION

Injectable polymer systems, as compared to preformed grafts, scaffolds, or hydroxyapatite blocks, are promising for tissue engineering applications due to multiple advantages such as controlled viscosity, shape adaptability to defect sites, tissue adhering ability during the stiffening process, and compatibility with a minimally invasive procedure.[1] With these unique properties, the injectable formulations may find applications in various tissue engineering applications, e.g., artificial cartilage, injected spine fusion, vertebroplasty, tooth enamel restoration, trabecular bone defect injection, and acetabulum injection.

The conventional injectable polymer systems, however, rely mostly on the utilizing of thiolene additions,[2, 3] double bonds,[4–12] or metal-catalyzed click reactions[13, 14] for crosslinking and stabilization. To initiate these reactions, radical initiators or photochemical irradiations and metal catalysts are required in the injectable formulation for the opening of reactive bonds and formation of the crosslinked polymer network. However, in most cases, these radical initiators and/or metal catalysts are extremely toxic or oxidative. The addition of these compounds generates unfavorable risks as they could cause damages to adjacent tissues or organs after released into blood circulation. These potential concerns largely limited the use of conventional injectable systems for clinical applications. To this end, an injectable system that is able to avoid the use of cytotoxic initiators or catalysts is therefore desired in regenerative medicine applications.

Strain-promoted alkyne-azide cycloaddition (SPACC) click chemistry is promoted by the energy in the stretched ring and thus free from initiators and catalysts.[15, 16] The reaction has gained extensive research interest due to unique orthogonality, excellent conversion efficiency, and favored biocompatibility.[17–20] To date, SPAAC click chemistry has been studied for applications such as hydrogel preparation,[21] microbubble functionalization,[22] peptides and surfactant synthesis,[23–25] targeted cell imaging or drug delivery,[26–29] and regenerative medicine.[30, 31] For example, a covalently cross-linked hydrogel was fabricated using SPAAC click reaction between poly(ethylene glycol) (PEG) terminated with dibenzocyclooctynol (DIBO) and glycerol exytholate triazide.[32] In another study, a hydrogel was fabricated within a minute using SPAAC click ligation of azadibenzocyclooctyne group with azide.[33] Moreover, SPAAC click was applied for DNA functionalization. For example, the DNA chains were reported to be ligated within one minute by SPAAC click reaction after functionalization with dibenzocyclooctyne (DBCO) groups.[34]

For the reconstruction of tissue defects or tissue engineering, various biodegradable polymers have been investigated in the past decades. For example, poly(ε-caprolactone) (PCL),[35–37] poly(caprolactone fumarate) (PCLF),[38] poly(ethylene glycol) (PEG),[39–41] oligo(poly(ethylene glycol)fumarate) (OPF),[42] poly(L-lactic acid) (PLLA),[43] poly(lactic-co-glycolic acid) (PLGA),[44] and poly(propylene fumarate) (PPF)[45] have been developed and explored *in vitro* or *in vivo* for tissue regeneration. PPF was developed to be biodegradable, mechanically strong, and supportive of bone cell adhesion, proliferation, and differentiation *in vitro* and tissue growth *in vivo*.[46–48] In the past years, our lab has developed and tested various copolymers or blends based on PPF polymer for bone regeneration and obtained promising results in both cell studies and animal implantations.[49]

In this study, we implemented the catalyst-free SPAAC click chemistry to the biodegradable PPF polymer and constructed an injectable PPF-BCN/hyPCL32-N_3 (PFCL-Click) system (Figure 1a) for tissue engineering and regenerative medicine, e.g., spine injection (Figure 1b). The strategy was realized by functionalization of PPF with BCN group to create a PPF-BCN polymer. Then a 32-arm hyper-branched PCL dendrimer terminated with azide group (hyPCL32-N_3) was developed as cross-linker, as demonstrated in Figure 1a. The rationale for developing a dendrimer structure with multiple arms is to increase functional group density and enhance the possibility for polymer chains to cross-link with each other. At the same time, linking multiple arms with a dendrimer core could minimize the possibility of generating un-cross-linked free chains and thus improve the biocompatibility of injectable scaffolds. For preformed scaffolds, they may receive pre-treatment steps, e.g., washing in acetone, which could remove the uncrosslinked sol part before implantation. However, for injectable systems, they are directly injected to the body without any further steps. The minimization of uncrosslinked polymer chains is critical for the success of injectable systems. The crosslinking ability, mechanical properties, surface hydrophilicity, protein adsorption, as well as degradation abilities of the polymer, were thoroughly characterized. The biocompatibility and thermal properties of PFCL-Click injectable system were compared with conventional PMMA bone cement. MC3T3 pre-osteoblast cell proliferation, spreading, and differentiation on the crosslinked PFCL-Click scaffolds were investigated. The injection ability and X-ray imaging ability of the PFCL-Click injectable system were also investigated.

2. MATERIALS AND METHODS

2.1 Materials

Chemicals including ε-caprolactone monomer, (1R,8S,9s)-Bicyclo[6.1.0]non-4-yn-9-ylmethanol (BCN-OH), hyperbranched bis-MPA polyester-32-hydroxyl, generation 3 (APL32-OH), tin(II) 2-ethylhexanoate ($Sn(Oct)_2$, 95%), sodium azide (NaN_3), and oxalyl chloride were purchased from Sigma Aldrich Co. (Milwaukee, WI) and used as received. Reagent grade solvents including acetone, dimethylformamide (DMF), and dichloromethane (DCM, CH_2Cl_2) were purchased from Fisher (Pittsburgh, PA). Anhydrous CH_2Cl_2 was obtained by distilling dichloromethane received from Fisher with calcium hydride (CaH_2) before use. Potassium carbonate (K_2CO_3) was purchased from Sigma Aldrich Co. (Milwaukee, WI) and dried in 100°C oven overnight to remove moisture residues. Other used reagents or chemicals, unless noted otherwise, were all purchased from either Fisher or Sigma and used as received.

2.2 Synthesis of PPF-BCN

The PPF-BCN was synthesized by reacting PPF terminated with hydroxyl groups with (1R,8S,9s)-Bicyclo[6.1.0]non-4-yn-9-ylmethanol chloride (BCN-COCOCl). PPF was synthesized according to a protocol as described previously.[45] To synthesize the reactive BCN-COCOCl intermediate, 150 mL CH_2Cl_2 was added to 4 Å molecular sieves and stirred under nitrogen gas to remove extra water. The flask was then transferred into an ice bath and added with 16 mL of oxalyl chloride. Then 0.4 g of (1R,8S,9s)-Bicyclo[6.1.0]non-4-yn-9-ylmethanol (BCN-OH) fully dissolved in 10 mL of CH_2Cl_2 was added slowly to the flask.

Excess amount (20 g) of anhydrous potassium carbonate (K_2CO_3) was then added to the flask as proton scavenger.

The reaction system was refluxed in 50°C oil bath for 4 hours with continuous stirring. Afterward, excess un-reacted oxalyl chloride and CH_2Cl_2 solvent were rotary evaporated overnight at 50 °C to collect BCN-COCOCl. Then 50 mL of anhydrous CH_2Cl_2 solvent was added into the flask to dissolve BCN-COCOCl followed by the addition of 10 g anhydrous potassium carbonate. PPF polymer (2.28 g) was first dissolved in 150 mL of anhydrous CH_2Cl_2 solvent and then added slowly into the flask. The reaction was kept under reflux in 50°C oil bath overnight with continuous stirring. Upon completion, the reaction system was centrifuged for 10 min at ~ 2060 *g* to precipitate K_2CO_3 solids. The supernatants containing polymers were concentrated by rotary evaporation, precipitated in excess diethyl ether, and dried under vacuum to obtain PPF-BCN. Dried PPF-BCN polymer was stored at −20 °C before use.

2.3 Synthesis of hyperbranched 32-arm hyPCL32-N_3 dendrimer

The hyPCL32-N_3 dendrimer was synthesized by a three-step procedure, i.e., hyPCL32-OH, hyPCL32-Br and then hyPCL32-N_3. To synthesis hyPCL32-OH dendrimer, 40 g of distilled pure ε-caprolactone was injected into a three-neck flask under nitrogen protection. A hyperbranched dendrimer core bis-MPA polyester-32-hydroxyl (APL32-OH, 0.45 g) was added afterwards as an initiator. Following the addition of a ring-opening catalyst, Tin(II) 2-ethyl hexanoate ($Sn(Oct)_2$, 0.16 g), the system was reacted for 12 hours under stirring at 140 °C in an oil bath. The obtained hyPCL32-OH dendrimer was cooled down to room temperature, precipitated three times in excess diethyl ether, then fully dried using pump vacuum.

To synthesize hyPCL32-Br, 20 g of hyPCL32-OH dendrimer was added into a three-neck flask together with 200 mL CH_2Cl_2 as solvent and 50 g of potassium carbonate as proton scavenger. The flask was then transferred to an ice bath and 2-bromopropionyl bromide (10 mL) was added dropwise under nitrogen gas. The reaction was maintained for 24 hours at room temperature under continuous stirring. After completion of the reaction, the system was centrifuged for 10 min at ~ 2060 *g* to remove K_2CO_3 solids, followed by precipitation in cold diethyl ether and dry in vacuum.

In the next step, 11.2 g of obtained hyPCL32-Br was reacted with 8.0 g of sodium azide with extreme caution (warning: sodium azide may cause explosion) for 24 hours at 90 °C in 200 mL dimethylformamide (DMF). After the reaction, the product was precipitated in a large amount of methanol, dissolved in acetone, and precipitated again. This purification process was repeated at least three times to remove sodium azide. The final hyPCL32-N_3 product was precipitated in cold diethyl ether then dried by pump vacuum. The dried hyPCL32-N_3 dendrimer was stored at −20 °C before use.

2.4 PFCL-Click scaffolds fabrication by SPAAC click chemistry

The injectable PFCL-Click formulation consisted of two components, which were prepared separately prior to crosslinking. For the PPF-BCN component, 0.5 g of synthesized PPF-BCN was dissolved in 0.25 mL of CH_2Cl_2. For the hyPCL32-N_3 component, 2.0 g of

synthesized hyPCL32-N_3 were dissolved in 1 mL of CH_2Cl_2. To evaluate the injection process, the two components were injected simultaneously into a glass vial to mimic the defect filling process.

The gelation time at both 37 °C and 60 °C was estimated using a tube inversion method according to previous references.[50–53] A prolonged overnight incubation (> 18 h) with cap open was conducted for thorough cross-linking of all components and evaporation of CH_2Cl_2 solvents in order to achieve cross-linked PFCL-Click dry specimens. For materials property evaluation, the two components were injected into a glass mold with silicone spacers and maintained at 37 °C overnight to obtain crosslinked PFCL-Click scaffolds.

2.5 Material characterizations

^{1}H nuclear magnetic resonance spectroscopy (NMR).—The chemical structures of synthesized PPF-BCN polymer and hyPCL32-N_3 dendrimer were dissolved in $CDCl_3$ solvent and characterized using 1H NMR spectroscopy (300 MHz Varian NMR).

Gel permeation chromatography (GPC).—The molecular weights of PPF-BCN and hyPCL32-N_3 were measured by gel permeation chromatography (GPC) using tetrahydrofuran (THF) as eluent on a 2410 refractive index detector equipped Viscotek GPCMax/VE 2001 GPC machine (Malvern Instruments, Inc.).

Swelling ratio and gel fraction.—After cross-linking, the PFCL-Click scaffolds were soaked in acetone or CH_2Cl_2 to determine the swelling ratio and gel fraction. Briefly, the specimen was weighed to record the original mass (W0). Then the specimens were placed in acetone or CH_2Cl_2 for 1 day to remove the uncrosslinked sol part and allow full swelling and then taken out to record swelled mass (Ws). After two days of drying under vacuum, the specimens were recorded for the final dry mass (Wd). The swelling ratio was calculated by the equation: Swelling ratio = (Ws – Wd)/Wd, and gel fraction was calculated using the equation: Gel fraction = 100% × Wd/W0. At least three specimens were tested and averaged for each study.

Mechanical properties.—The compressive mechanical strength of crosslinked PFCL-Click scaffold was tested using a dynamic mechanical analyzer (DMA) (RSA-G2, TA instruments) with strain rate set at 0.001 mm/s. The compressive moduli of PFCL-Click specimens were calculated from the stress-strain curve in the linear region.

Dynamic mechanical frequency sweep test.—Storage and loss moduli were measured by performing a frequency sweep on a TA Instruments RSA-G2 dynamic mechanical analyzer. A strain rate of 0.02% at an angular frequency range from 0.1 rad/s to 100 rad/s (~ 0.16 Hz −15.92 Hz) was applied and storage and loss moduli were determined at 10 points per decade.

Degradation properties.—Accelerated degradation of crosslinked PFCL-Click scaffolds was performed in 0.1 M NaOH and 0.01 M NaOH solutions. The remaining mass of the PFCL-Click scaffolds immersed in the solution was recorded each week during the first 4 weeks and measured every other week thereafter until the scaffolds fully disappeared. The

long-term degradation of crosslinked PFCL-Click scaffolds in simulated body fluids was also evaluated. Specimens were immersed in phosphate-buffered saline (PBS) solution and the remaining weight was recorded each week during the first 4 weeks and measured every two weeks thereafter until 18 weeks.

Surface wettability and protein adsorption.—To analyze the protein adsorption ability of the PFCL-Click scaffolds, the specimens were immersed in cell culture medium supplemented with 10% fetal bovine serum (FBS) at 37 °C for 0.5 hour or 2.0 hours. After the immersion, specimens were washed three times with PBS to eliminate non-adsorbed surface residue proteins. The proteins adsorbed on the PFCL-Click scaffolds were collected by washing with 1% sodium dodecyl sulfate (SDS, Bio-Rad Laboratories, Inc.). MicroBCA protein assay kit (Pierce, Rockford, IL) were used for protein analysis using a standard curve generated by known concentrations of albumin solutions. Optical density (OD) values of adsorbed proteins were determined on a microplate reader (SpectraMax Plus 384, Molecular Devices, Sunnyvale, CA) and the protein quantities were determined by the above standard curve.

2.6 Live/dead staining and cytotoxicity of pre-osteoblast cells on scaffolds

Before seeding, MC3T3 pre-osteoblast cells were maintained in the non-osteogenic state in ascorbic acid-free α-Minimum Essential Medium (α-MEM) supplemented with 10% FBS and 0.5% streptomycin/penicillin. For the live/dead study, the PFCL-Click scaffolds were sterilized by immersing in 70% alcohol solution overnight and washed with sterilized PBS for at least five times. MC3T3 cells were trypsinized, counted, and seeded onto the sterilized PFCL-Click scaffolds at a density of 15, 000 cells per cm^2. After 1 day of culture on the scaffold, the cells were stained with LIVE/DEAD® Cell Imaging Kit (Thermo Fisher Scientific, Waltham, MA) and imaged on an Axiovert 25 Zeiss light microscope (Carl Zeiss, Germany). The clinically used PMMA scaffolds were used as a control group for the live/dead staining following the same protocol.

To further confirm the cytocompatibility of the scaffold, MC3T3 pre-osteoblast cells were seeded at a density of 15, 000 cells per cm^2 in six-well tissue culture polystyrene (TCPS) plates. The crosslinked PFCL-Click scaffolds and clinically used PMMA scaffolds were put in transwell chambers (mesh size 3 μm) and inserted into the six-well TCPS plates with medium covering the specimens. After 1, 3, and 5 days of culture, the cell viability in each TCPS well was determined using the MTS assay. Cell viability rate was calculated using the TCPS wells without transwell inserts as a positive control (set as 100%).

2.7 Pre-osteoblast cell proliferation on PFCL-Click scaffolds

The crosslinked PFCL-Click scaffolds were sterilized by immersing in 70% alcohol solution overnight and then washed at least five times with sterile PBS. After drying, the crosslinked PFCL-Click scaffolds were adhered to the bottom of 48-well TCPS plates using silicon-based vacuum grease. MC3T3 cells were diluted in α-MEM and seeded on the crosslinked PFCL-Click scaffolds at a density of 15 000 cells cm^{-2}. The cells were then cultured in the incubator at 95% relative humidity, 5% CO_2, and 37 °C. At 1, 3, and 5 days post-seeding, the α-MEM media were removed and the crosslinked PFCL-Click specimens were

rinsed with PBS to wash away unattached cells. Cell numbers on the crosslinked PFCL-Click specimens were quantified by the MTS assay (CellTiter 96, Promega, Madison, WI) according to the kit protocols. The absorbance of MTS solution from each specimen was read by UV-vis absorbance microplate reader (SpectraMax Plus 384, Molecular Devices, Sunnyvale, CA) at a wavelength of 490 nm.

2.8 Osteogenic differentiation of MC3T3 on PFCL-Click scaffolds

For osteogenic differentiation of MC3T3 pre-osteoblast cells, the α-MEM medium was supplemented with 10% fetal bovine serum, 0.5% streptomycin/penicillin, 10 mM β-glycerophosphate (β-GP), and 50 μg/mL ascorbic acid (AA). Prior to seeding, MC3T3 pre-osteoblast cells were maintained in the non-osteogenic state in ascorbic acid-free α-MEM. The crosslinked PFCL-Click scaffolds were sterilized with 70% alcohol solution, washed with PBS, and attached to the 48-well TCPS plates using silicon-based vacuum grease, as stated above. MC3T3 cells were diluted in α-MEM and seeded to the crosslinked PFCL-Click scaffolds at a density of 15 000 cells cm^{-2}. The plates were kept in 37 °C incubator for 4 hours to allow attachment of cells to the PFCL-Click scaffolds. Then the α-MEM medium was removed and replaced with the α-MEM/β-GP/ AA osteogenic medium and cultured in the 37 °C incubator. At 1, 3, and 5 days post-seeding, the α-MEM/β-GP/ AA medium was removed, and cell numbers on the crosslinked PFCL-Click specimens were quantified by the MTS assay as stated above.

2.9 Immuno-fluorescence staining and imaging

To image the MC3T3 cellular morphologies on the crosslinked PFCL-Click scaffolds, cells grown on the samples were fixed for 10 min in 4% paraformaldehyde solution. Cells were then washed with PBS three times and treated for 10 min in 0.2% Triton X-100 to permeabilize the cell membrane. Fixed cells were then stained with rhodamine-phalloidin (RP, Cytoskeleton Inc) at 37 °C for 60 min to label cellular filaments. Labeled cells were incubated in 4’,6-diamidino-2-phenylindole (DAPI) solution for 10 min at 37 °C to stain cell nuclei. Fluorescence-labeled MC3T3 cells were imaged on an Axiovert 25 Zeiss light microscope (Carl Zeiss, Germany).

For confocal imaging of MC3T3 cellular morphologies after differentiation in the osteogenic medium on the crosslinked PFCL-Click scaffolds, cells were fixed and permeabilized as stated above. Prior to immuno-fluorescence staining, specimens with fixed MC3T3 cells were treated in 37 °C PBS solution containing 1% bovine serum albumin (BSA) to block non-specific binding sites. After washing for 3 times with PBS, cells on PFCL-Click specimens were then incubated for 1 h with anti-vinculin–FITC antibody (Sigma-Aldrich Co., Milwaukee, WI) at 37 °C to label vinculin, the main compound for cell focal adhesions. After the incubation, cells were further stained with RP to label F-actin arrangement and with DAPI to label cell nuclei, similar to the above procedures. The immune-fluorescence stained MC3T3 cells on the crosslinked PFCL-Click scaffolds were instantly imaged on an inverted laser scanning confocal microscope (Carl Zeiss, Germany). Cell area, cell circularity, nuclei area, and nuclei circularity of the cells were analyzed using the ImageJ software (National Institutes of Health).

2.10 Alkaline phosphatase, osteocalcin, and collagen production

Alkaline phosphatase (ALP) activity.—To extract the intracellular alkaline phosphatase, the crosslinked PFCL-Click scaffolds with MC3T3 cells were washed thoroughly with PBS to eliminate non-adhered cells. Cells growing on the crosslinked PFCL-Click scaffolds were trypsinized and collected in a 50 mL tube. The cell suspensions were centrifuged and repeatedly washed with sterile de-ionized H_2O for at least 5 times. After counting, the cells were lysed using 0.2% Triton X-100 (0.5 mL solution per 1 $\times 10^4$ cells) overnight at 4 °C. The alkaline phosphatase activity in the lysate solutions was determined using an Alkaline Phosphatase Assay Kit (QuantiChromeTM, BioAssay Systems, Hayward, CA).

Osteocalcin (OC).—For osteocalcin determination, the MC3T3 pre-osteoblast cell culture medium was collected as described in a previous study.[54] The osteocalcin concentration in the medium was determined using a quantitative Mouse Osteocalcin Enzyme Immunoassay Kit (Alfa Aesar, Thermo Fisher Scientific). The OD value was read at 450 nm and concentration was calculated using a standard curve generated with known concentrations according to the kit protocol.

Collagen production.—The total cellular collagen production of MC3T3 cells on the PFCL-Click scaffolds was determined by the Sirius red staining method.[55, 56] Before staining, the PFCL-Click scaffolds were rinsed with PBS and MC3T3 cells grown on the surface were fixed using 4% paraformaldehyde aqueous solution. Sirius red stain solution was prepared by mixing 0.1% Direct Red 80 into saturated picric acid (Sigma-Aldrich). After placing into 24-well TCPS plates, crosslinked PFCL-Click scaffolds with cells were stained with 1 mL of Sirius red stain solution for 16 hours. Stained scaffolds were then washed with distilled water, dehydrated using 100% ethanol, dried in vacuum, and weighed to record dried mass (Wm) of each specimen. The stain on each sample was then eluted by washing with 1 mL of 0.2 M NaOH: methanol (v/v, 1: 1) solution for 15 min. The absorbance of the eluted solution was read by a microplate reader at 490 nm then divided by dried mass (Wm) to obtain the absorbance per gram of scaffolds.

2.11 Rabbit spine defect injection and X-ray imaging

To show the injection capability and ability to be visualized by X-ray, the ZrO_2 powder was added as an X-ray contrast agent to the PFCL-Click injectable system and rabbit vertebral body was used as a defect model. Before injection, the PPF-BCN and hyPCL32-N_3 were combined with ZrO_2 power (10% to polymer weight) and then dissolved in CH_2Cl_2 solvent in two separate syringes, as described in the above section. Rabbit spines were extracted and cleaned of excess soft tissue. A small hole was drilled on each of the lateral sides of the rabbit vertebral body to expose the marrow cavity. The marrow was then excavated to leave a cavity for the injection of cement. The PPF-BCN/hyPCL32-N_3/ZrO_2 mixed resin was then injected into the defect. After injection, the spines were incubated at body temperature of 37 °C overnight to allow crosslinking of polymers through SPAAC click chemistry. After the reaction, the rabbit spines were imaged using a cabinet X-ray system (Faxitron X-ray Corporation, Tucson, Arizona). Clinically used PMMA (Coltene/Whaledent, Inc., Cuyahoga Falls, OH) served as a control group for the injection study.

2.12 Statistical analysis

A one-way analysis of variance (ANOVA) followed by Tukey post-test was performed for the statistical analysis of data. Any two groups that were calculated with $p < 0.05$ were marked as significantly different.

3. RESULTS AND DISCUSSION

3.1 PPF-BCN and hyPCL32-N_3 synthesis and crosslinking

The two polymer components with clickable tails were synthesized by a facile route, as demonstrated in Figure 2a–b. The chemical structures of the synthesized PPF-OH, PPF-BCN polymer were confirmed with ^{1}H NMR spectroscopy using $CDCl_3$ solvent (Figure S1). GPC results showed that the resulting PPF-BCN polymer had a number average molecular weight (M_n) of 1692 g mol^{-1}, a weight average molecular weight (M_w) of 4210 g mol^{-1}, and a polydispersity index (PDI) of 2.5. The synthesized hyPCL32-N_3 dendrimer was confirmed by ^{1}H NMR spectroscopy (Figure S2). GPC showed the hyPCL32-N_3 dendrimer had an M_n of 112,689 g mol^{-1}, M_w of 375,635 g mol^{-1}, and a PDI of 3.3. Obtained polymers were all dried in vacuum and stored at −20 °C before use.

Prior to crosslinking, the PPF-BCN polymers and the hyPCL32-N_3 dendrimers were dissolved in CH_2Cl_2 solvent in separate vials. To measure the cross-linkability, the two polymer solutions were mixed thoroughly and injected into a glass vail mimicking the tissue defect (Figure 3a). After incubation at 37 °C for a certain amount of time, the mixture successfully gelled due to the linkage caused by SPAAC click reaction between the alkyne end on PPF-BCN and the azide end on hyPCL32-N_3 dendrimer (Figure 3a). The gelation time of the PFCL-Click injectable system varied depending on several parameters including the concentration and ratio of the two components and reaction temperature. Through an extensive investigation, we found that the 1:4 wt/wt ratio of PPF-BCN and hyPCL32-N_3 resulted in the best crosslinking. The gelation time of the injectable system at body temperature of 37 °C, as well as a higher temperature of 60 °C, were investigated. Results showed that the PFCL-Click injectable system started to gel within 15.5 ± 3.5 min at 37 °C, due to the SPAAC click reaction between the BCN tail and the azide tail of the two polymer components (Figure 3a–b). Under higher temperature of 60 °C, the gelation time shorted to 6.5 ± 2.1 min, mainly because of the enhanced reaction rate for the SPAAC click reaction at a higher temperature. Further overnight incubation with the cap open (or in an open container) was necessary for full cross-linking and solvent evaporation in order to obtain cross-linked PFCL-Click dry specimens.

3.2 Gel fraction, protein adsorption and mechanical properties

The cross-linked PFCL-Click dry specimens were immersed in CH_2Cl_2 and acetone to determine the swelling ratio and gel fraction. Results showed that the cross-linked PFCL-Click specimens swelled but did not dissolve in organic solvents. This indicates a successful cross-linking between the PPF-BCN and hyPCL32-N_3 components. The gel fraction and swelling ratio in acetone were determined to be 90.4 ± 3.2% and 10.7 ± 5.4, respectively (Figure 3c–d). In the CH_2Cl_2 solvent, the gel fraction and swelling ratio were determined with similar values of 87.2 ± 5.9% and 11.3 ± 3.3, respectively (Figure 3c–d).

The mechanical properties of the cross-linked PFCL-Click dry specimens were measured on a DMA with strain rate set as 1×10^{-4} mm/s. Compressive modulus was calculated to be 16.6 ± 5.6 MPa (Figure 3e), from the linear region of the compressive stress-strain curve (Figure 3f). A dynamic mechanical frequency sweep test on crosslinked PFCL-Click scaffolds was conducted at varying frequencies from 0.1 rad/s to 100 rad/s (~ 0.16 Hz −15.92 Hz). The changes in storage modulus (G'), as well as loss modulus (G''), were recorded and plotted against varied frequencies. As seen from Figure 3g, a stiffer behavior was observed with the increase of applied frequency. This is because higher frequency leads to less response time for polymer chain movements and thus “freezes” the polymer network to result in a stronger mechanical stiffness.

High load-bearing bones like trabecular bone, femur, and spine vertebral body, have modulus from hundreds of megapascals (MPa) to several gigapascals (GPa).[57, 58] We have previously developed injectable and preformed PPF polymer systems that could reach modulus in this level satisfying the high load-bearing requirement.[7, 59, 60] For this PFCL-Click injectable system, based on the mechanical strength with modulus of 16 MPa, is mainly suitable for low load-bearing tissue applications, e.g., artificial cartilage, injected spine defect filling, tooth enamel restoration, trabecular bone defect injection, and acetabulum injection.

Surface and internal morphologies of crosslinked PFCL-Click scaffolds were examined by SEM after drying. As shown in Figure 3h, a flat surface with porous structures densely distributed on the surface was observed. The internal structure revealed after breaking down the scaffold also demonstrated sparsely distributed pores within the scaffolds. These porous structures were believed to result from the evaporation of the solvent, i.e., dichloromethane, during the sequential crosslinking process. The thermogravimetric analysis demonstrated that the crosslinked PFCL-Click scaffolds started drastic mass loss at a temperature higher than 350 °C, as shown in Figure 3i. Under physiological condition, both the PPF and PCL segments in the cross-linked PFCL-Click scaffolds can be cleaved by hydrolysis of the ester bonds in the polymer chain, rendering the cross-linked PFCL-Click scaffolds biodegradable. An accelerated degradation study of crosslinked PFCL-Click scaffold showed that scaffolds disappeared completely in 6 weeks in 0.1 M NaOH (Figure 3j). In a milder condition of 0.01 M NaOH, the crosslinked PFCL-Click scaffold reduced masses more gradually before totally disappeared at 12 weeks.

In a simulated physiological PBS condition, the crosslinked PFCL-Click scaffold showed fairly slow degradation with 92.6 ± 3.2% weight remaining at the end of the observation period of 18 weeks. After biodegradation of polymer chains into small segments (< 3000 Da), it was reported that cellular uptake may occur and the scaffolds can be completely biodegraded after certain period of time via the intracellular mechanism.[61] Protein adsorption test showed continuous adsorption of proteins to the surface of the crosslinked PFCL-Click scaffold with increased numbers of 4.7 ± 2.1 μg/cm^2 and 10.5 ± 3.2 μg/cm^2 at 0.5 hour and 2 hours soaking in cell culture medium (Figure 3k).

3.3 Thermal -behavior and biocompatibility

After overnight reaction at 37 °C, the crosslinked PFCL-Click scaffolds were successfully fabricated. As presented in Figure 4a, the PFCL-Click scaffolds showed light yellowish opaque appearance. The temperature change during the crosslinking process was recorded using a thermometer. As presented in Figure 4b, the PFCL-Click injectable system showed minimal heat generation during the crosslinking process. As a comparison, the clinically used PMMA showed significant heat generation with temperature rising to over 80 °C. This high temperature is not suitable for potential protein incorporation within the PMMA. However, for our PFCL-Click injectable system, the mild reaction temperature would allow for encapsulation of proteins such as bone morphogenetic protein-2 (BMP-2) to induce bone formation and tissue regeneration.

After crosslinking, the surface wettability test showed PFCL-Click scaffold was highly hydrophobic, similar to the PMMA scaffold (Figure 4c–d). The wettability of a biomaterial's surface was reported to be critical for protein adhesion.[62] Hydrophobic surfaces with contact angles larger than 60 degree is determined to have excellent protein adsorption.[62] As demonstrated in Figure 4c–d, the PFCL-Click scaffolds showed strong hydrophobic surfaces with contact angles around 80 degrees at the initial stage and eventually reached values above 65 degrees. This indicates that the PFCL-Click scaffold is preferable for protein adsorption, further confirms the robust protein adsorption results in Figure 3k.

Live/dead cell viability test showed a larger portion of dead cells on the PMMA scaffolds, while a majority of the cells on the crosslinked PFCL-Click scaffold remained alive (Figure 4e–g). This may be because the crosslinked PFCL-Click scaffold eliminated the use of toxic crosslinking reagents and thus showed better cell viability compared to the PMMA bone cement, which used toxic benzoyl peroxide (BPO) as an initiator and N-dimethyl toluidine (DMT) as an accelerator for crosslinking. The cytotoxicity test by MTS assay further confirmed better cytocompatibility for crosslinked PFCL-Click scaffold compared to PMMA (Figure 4h). Therefore, the crosslinked PFCL-Click scaffold is regarded to have suitable biocompatibility for tissue engineering.

3.4 Proliferation of MC3T3 pre-osteoblast cells on PFCL-Click scaffolds

To determine the ability of the crosslinked PFCL-Click scaffolds to support cell attachment and proliferation, MC3T3 cells were seeded on the scaffolds placed in 48-well tissue culture plates and the cell numbers were measured by the MTS assay. As presented in Figure 5a, the OD values showed an increasing trend at 1, 3, and 5 days post-seeding, indicating that cell expansion on the scaffolds. Statistical analysis showed a significant growth ($p < 0.05$) of cell densities at 3 and 5 days post-seeding compared to cells at day 1 on the crosslinked PFCL-Click scaffolds (Figure 5a). After fixation, the cells were stained with immune-fluorescence rhodamine-phalloidin and DAPI makers and imaged. As demonstrated in Figure 5b, the cell numbers counted from the fluorescence images showed a similar growth trend to the MTS assay, which further confirmed that crosslinked PFCL-Click scaffolds supported cell proliferation.

The spreading areas of MC3T3 cells at 1, 3, 5 days post-seeding on the scaffolds were measured and the distributions of 20 typical cell areas were displayed in Figure 5c. The average spreading areas of MC3T3 cells post-seeding were calculated to have increasing values with prolonged culturing time from 1 day to 3 and 5 days. Typical images of cell morphologies at 1, 3, and 5 days growing on the scaffolds were presented in Figure 5d and Figure S3. As can be seen from the images, the cells developed robust filaments and nuclei after 3 days of culture, demonstrating healthy cellular activities on these crosslinked PFCL-Click scaffolds.

The cell circularity, defined by $4\pi \times \text{area/perimeter}^2$, is measured by ImageJ software to describe cell shape. The circularity value for a perfect circle is 1.0 and for a line 0.0. Therefore, cells with round shape will have higher circularity values closer to 1.0 whereas cells with linear shapes will have decreased values closer to 0.0. As can be noticed from Figure 5e, the circularity of MC3T3 cells dropped at 1, 3, 5 days post-seeding, indicating the cells were spreading and stretched to a more linear shape. The cell nuclei were determined to have the highest spreading area and lowest circularity at 3 days post-seeding, as shown in Figure 5f–g. This may indicate that the cells had the most robust dividing and expansion kinetics at day 3 of culture on the scaffolds. This result can also be explained that the cells were adjusting to the new cell environment at 1 day of seeding onto the scaffolds, while at 5 days post-seeding, cells were already reaching relative confluency on the scaffolds thus the division activities may be reduced accordingly.

3.5 Osteogenic medium induced cell behavior on PFCL-Click scaffolds

To evaluate cellular behavior on the crosslinked PFCL-Click scaffolds under osteogenic differentiation, the MC3T3 pre-osteoblast cells were first seeded to the scaffolds. After attachment, the medium was changed into osteogenic medium supplemented with 10 mM β-glycerophosphate (β-GP) and 50 μg/mL ascorbic acid (AA). At 1, 3, and 5 days post-seeding, cell numbers on the crosslinked PFCL-Click scaffolds cultured in α-MEM/β-GP/AA osteogenic medium were quantified by the MTS assay using TCPS as positive control.

As presented in Figure 6a, the cell numbers gradually increased, indicating proliferation of MC3T3 cells on scaffolds in the osteogenic medium. However, the OD values were determined to be slightly lower that of cells growing in the non-osteogenic medium. This may imply that cell proliferation was inhibited slightly by the osteogenic differentiation medium. Cell area, cell circularity as well as nuclei area and nuclei circularity were thoroughly analyzed. As can be noted from Figure 6b and Figure S4a, the cell area and circularity were similar to those cultured in the non-osteogenic medium. However, for cell nuclei, a slight difference was determined with the highest area and lowest nuclei circularity to occur at 5 days post-seeding (Figure 5c and Figure S4b), instead of at 3 days post-seeding for cells cultured in the non-osteogenic medium. This may be caused by the slower growth rate which altered the nuclei activity and postponed the peak activity for nuclei to day 5 post-seeding.

Confocal images of cellular morphologies after 1, 3, and 5 days of cell culture on the scaffolds were demonstrated in Figure 6d. As noticed from the images, the cells developed

robust filaments, as well as strong focal adhesions. A 3-D depth scanning of cell layers was conducted using a confocal microscope to show cell layer thickness. As can be seen from the 3D reconstruction images in Figure 6e–g, MC3T3 cells proliferated and occupied more and more spaces on the surface of the crosslinked PFCL-Click scaffolds. At 1 day post-seeding, the cells occupied only less than half of the surface. After 3 days of growth, the cells occupied the majority of the PFCL-Click scaffold surface with 1 cell layer from the Z-axis view. After 5 days of growth, the cells occupied almost the entire PFCL-Click scaffold surface with approximately 2 cell layer thickness from the Z-axis view. These results all indicated that crosslinked PFCL-Click scaffolds were excellent in supporting cell adhesion and proliferation.

3.6 ALP, OCN, collagen production and rabbit spine injection

To evaluate the osteogenic differentiation ability of MC3T3 pre-osteoblasts cells on the crosslinked PFCL-Click scaffolds, changes in intracellular ALP and OCN were analyzed after 1, 2 and 3 weeks of culture using current clinically used PMMA as a positive scaffold control. As presented in Figure 7a, the ALP levels in MC3T3 cells cultured in non-osteogenic α-MEM increased to more than 3 folds at 2 and 3 weeks, as compared to week 1. The OCN increased to around 3 folds and eventually 5 folds as compared to week 1 on the crosslinked PFCL-Click scaffolds. This significant increase in the differentiation markers in MC3T3 pre-osteoblasts cells indicated that the crosslinked PFCL-Click scaffolds were able to support the osteogenic differentiation of cells. Total collagen analysis showed a drastic enrichment of collagens on the scaffolds, indicating cells were producing the essential amount of extracellular matrix (ECM) on these PFCL-Click scaffolds.

To further investigate the differentiation profile of cells after osteogenic induction, cells were cultured in α-MEM medium supplemented with 10 mM β-glycerophosphate and 50 μg/mL ascorbic acid. The intracellular ALP and OCN were analyzed at 1, 2 and 3 weeks of culture. As can be noted from Figure 7d, after induction, the ALP level increased to around 17 folds at 2 weeks and 15 folds at 3 weeks culture, as compared to week 1. The OCN level also jumped to more than 6 and 9 folds as compared to week 1. All these results indicate that the MC3T3 pre-osteoblasts cells underwent accelerated osteogenic differentiation after induction by the α-MEM/β-GP/AA medium on the crosslinked PFCL-Click scaffolds. Total collagen production, however, reduced slightly compared to the levels in cells cultured in non-osteogenic α-MEM medium. This indicates that the α-MEM/β-GP/AA osteogenic medium induced the osteogenic differentiation of MC3T3 cells while slightly reduced the proliferation of the cells. The ALP activities, OCN contents, and total collagen production on the PFCL-Click scaffolds were similar to those of the current clinically used PMMA scaffolds. All these results indicate that the PFCL-Click scaffolds were able to support extracellular matrix development and osteogenic differentiation of MC3T3 pre-osteoblast cells.

To show the injection ability and X-ray imaging ability, the PFCL-Click injectable system were thoroughly mixed with ZrO_2 power using two syringes (Figure 7g). Rabbit vertebral bodies were extracted and created cavities for cement injection, as demonstrated in Figure 7g and Figure S5. The mixed system was then injected to the cavities in the rabbit vertebral

bodies. Clinically used PMMA bone cement served as a control group for the injection study. As can be seen from X-ray images in Figure 7h, PFCL-Click injectable system was able to fill the cavity and could be monitored by X-ray imaging, similar to PMMA. Therefore, with the injection capability and monitoring ability, the PFCL-Click injectable system is promising for broad applications in tissue engineering including bone fracture injection, vertebroplasty, and spinal fusions.

The PMMA bone cement has been approved by the Food and Drug Administration (FDA) and is safe to use clinically as a bone void filler. PMMA uses methyl methacrylate (MMA) as the solvent, while the PFCL injectable system developed in this study uses dichloromethane (DCM), which is recognized by the World Health Organization (WHO) to have relatively low acute toxicity compared to MMA.[63–65] In addition, the Immediately Dangerous to Life or Health (IDLH) concentration for MMA is as low as 1,000 ppm for humans.[66] In comparison, the IDLH for DCM is set for 2,300 ppm, much higher than MMA.[67, 68] Thus, DCM is less toxic to the human body than MMA at the same amount. Therefore, the PFCL injectable system is expected to be biocompatible and safe to use as a bone void filler.

After crosslinking, there might be slight shrinkage of the scaffold caused by solvent evaporation. However, since we will incorporate porogens at greater than 70% v/v in order for the injected scaffold to be highly porous, the shrinkage of the scaffold is expected to be minimal and will have little effect on the space-filling capacity of the scaffold. Following hydrolysis of the ester bonds in the polymer backbone, the injected scaffold will be gradually degraded and new bone will eventually fill up the void space.[69, 70] Further animal and clinical studies are needed to confirm the biocompatibility and bone regeneration capacity of the injectable PFCL system.

CONCLUSIONS

In summary, we have developed a novel PFCL-Click injectable polymeric formulation capable of self-crosslinking using metal-free click chemistry for broad tissue engineering applications. The crosslinking between the two components in the injectable system was determined to proceed effectively via SPAAC click reaction without the requirement of any toxic initiators, accelerators, or catalysts. Gel fraction and swelling ratio tests showed excellent crosslinking ability for the system. Mechanical testing showed the crosslinked scaffold had relatively strong compressive strength and was suggested for low load bearing applications in tissue engineering. Degradation studies showed the systems can be degraded by simple hydrolysis. As compared to the conventional injectable formulations such as PMMA bone cement, the PFCL-Click injectable system developed in this study excluded the use of toxic initiator and catalyst and generated minimal heat during crosslinking, thus granting the system excellent biocompatibility. Cell studies further showed that crosslinked PFCL-Click scaffolds supported excellent MC3T3 pre-osteoblast cell proliferation, spreading, and differentiation. After incorporating ZrO_2 powder, the PFCL-Click injectable system could be monitored by X-ray imaging following successful injection to the defected vertebral bodies in the rabbit spine. With these advantages, this

injectable polymeric system holds great promise for broad applications in tissue engineering and regenerative medicine.

Supplementary Material

Refer to Web version on PubMed Central for supplementary material.

ACKNOWLEDGMENTS

This work was supported by National Institutes of Health grant R01 AR56212 and R01 AR075037.

REFERENCES

1. Salgado CL; Sanchez EM; Zavaglia CA; Almeida AB; Granja PL, Injectable biodegradable polycaprolactone-sebacic acid gels for bone tissue engineering. Tissue Eng Part A 2012, 18 (1–2), 137–46. [PubMed: 21902607]
2. Salinas CN; Anseth KS, Mixed mode thiol-acrylate photopolymerizations for the synthesis of PEG-peptide hydrogels. Macromolecules 2008, 41 (16), 6019–6026.
3. Daniele MA; Adams AA; Naciri J; North SH; Ligler FS, Interpenetrating networks based on gelatin methacrylamide and PEG formed using concurrent thiol click chemistries for hydrogel tissue engineering scaffolds. Biomaterials 2014, 35 (6), 1845–1856. [PubMed: 24314597]
4. Payne RG; Yaszemski MJ; Yasko AW; Mikos AG, Development of an injectable, in situ crosslinkable, degradable polymeric carrier for osteogenic cell populations. Part 1. Encapsulation of marrow stromal osteoblasts in surface crosslinked gelatin microparticles. Biomaterials 2002, 23 (22), 4359–4371. [PubMed: 12219826]
5. Jabbari E; Wang SF; Lu LC; Gruetzmacher JA; Ameenuddin S; Hefferan TE; Currier BL; Windebank AJ; Yaszemski MJ, Synthesis, material properties, and biocompatibility of a novel self-cross-linkable poly(caprolactone fumarate) as an injectable tissue engineering scaffold. Biomacromolecules 2005, 6 (5), 2503–2511. [PubMed: 16153086]
6. Kim C; Mahar A; Perry A; Massie J; Lu LC; Currier B; Yaszemski MJ, Biomechanical evaluation of an injectable radiopaque polypropylene fumarate cement for kyphoplasty in a cadaveric osteoporotic vertebral compression fracture model. J Spinal Disord Tech 2007, 20 (8), 604–609. [PubMed: 18046174]
7. Kim CW; Talac R; Lu LC; Moore MJ; Currier BL; Yaszemski MJ, Characterization of porous injectable poly-(propylene fumarate)-based bone graft substitute. J Biomed Mater Res A 2008, 85a (4), 1114–1119.
8. Yan J; Li JM; Runge MB; Dadsetan M; Chen QS; Lu LC; Yaszemski MJ, Cross-linking Characteristics and Mechanical Properties of an Injectable Biomaterial Composed of Polypropylene Fumarate and Polycaprolactone Co-polymer. Journal of Biomaterials Science-Polymer Edition 2011, 22 (4–6), 489–504. [PubMed: 20566042]
9. Fang Z; Giambini H; Zeng H; Camp JJ; Dadsetan M; Robb RA; An KN; Yaszemski MJ; Lu LC, Biomechanical Evaluation of an Injectable and Biodegradable Copolymer P(PF-co-CL) in a Cadaveric Vertebral Body Defect Model. Tissue Engineering Part A 2014, 20 (5–6), 1096–1102. [PubMed: 24256208]
10. Mihaila SM; Gaharwar AK; Reis RL; Marques AP; Gomes ME; Khademhosseini A, Photocrosslinkable Kappa-Carrageenan Hydrogels for Tissue Engineering Applications. Advanced Healthcare Materials 2013, 2 (6), 895–907. [PubMed: 23281344]
11. Paul A; Hasan A; Al Kindi H; Gaharwar AK; Rao VTS; Nikkhah M; Shin SR; Krafft D; Dokmeci MR; Shum-Tim D; Khademhosseini A, Injectable Graphene Oxide/Hydrogel-Based Angiogenic Gene Delivery System for Vasculogenesis and Cardiac Repair. Acs Nano 2014, 8 (8), 8050–8062. [PubMed: 24988275]
12. Li YQ; Liu W; Liu F; Zeng Y; Zuo SM; Feng SY; Qi CX; Wang BJ; Yan XJ; Khademhosseini A; Bai J; Du YA, Primed 3D injectable microniches enabling low-dosage cell therapy for critical limb

ischemia. Proceedings of the National Academy of Sciences of the United States of America 2014, 111 (37), 13511–13516. [PubMed: 25197069]

13. Nimmo CM; Shoichet MS, Regenerative biomaterials that “click”: simple, aqueous-based protocols for hydrogel synthesis, surface immobilization, and 3D patterning. Bioconjug Chem 2011, 22 (11), 2199–209. [PubMed: 21995458]
14. van Dijk M; van Nostrum CF; Hennink WE; Rijkers DT; Liskamp RM, Synthesis and characterization of enzymatically biodegradable PEG and peptide-based hydrogels prepared by click chemistry. Biomacromolecules 2010, 11 (6), 1608–14. [PubMed: 20496905]
15. Sletten EM; Bertozzi CR, From mechanism to mouse: a tale of two bioorthogonal reactions. Acc Chem Res 2011, 44 (9), 666–76. [PubMed: 21838330]
16. Jewett JC; Bertozzi CR, Cu-free click cycloaddition reactions in chemical biology. Chem Soc Rev 2010, 39 (4), 1272–1279. [PubMed: 20349533]
17. Deforest CA; Sims EA; Anseth KS, Peptide-Functionalized Click Hydrogels with Independently Tunable Mechanics and Chemical Functionality for 3D Cell Culture. Chem Mater 2010, 22 (16), 4783–4790. [PubMed: 20842213]
18. Zhang W; Huang M; Su H; Zhang S; Yue K; Dong XH; Li X; Liu H; Zhang S; Wesdemiotis C; Lotz B; Zhang WB; Li Y; Cheng SZ, Toward Controlled Hierarchical Heterogeneities in Giant Molecules with Precisely Arranged Nano Building Blocks. ACS Cent Sci 2016, 2 (1), 48–54. [PubMed: 27163025]
19. Gordon CG; Mackey JL; Jewett JC; Sletten EM; Houk KN; Bertozzi CR, Reactivity of biarylazacyclooctynones in copper-free click chemistry. J Am Chem Soc 2012, 134 (22), 9199–208. [PubMed: 22553995]
20. DeForest CA; Polizzotti BD; Anseth KS, Sequential click reactions for synthesizing and patterning three-dimensional cell microenvironments. Nat Mater 2009, 8 (8), 659–64. [PubMed: 19543279]
21. DeForest CA; Anseth KS, Cytocompatible click-based hydrogels with dynamically tunable properties through orthogonal photoconjugation and photocleavage reactions. Nat Chem 2011, 3 (12), 925–31. [PubMed: 22109271]
22. Liu X; Gong P; Song P; Xie F; Miller II AL; Chen S; Lu L, Fast functionalization of ultrasound microbubbles using strain promoted click chemistry. Biomater Sci-Uk 2018, 6 (3), 623–632.
23. Li YW; Wang Z; Zheng JK; Su H; Lin F; Guo K; Feng XY; Wesdemiotis C; Becker ML; Cheng SZD; Zhang WB, Cascading One-Pot Synthesis of Single-Tailed and Asymmetric Multitailed Giant Surfactants. Acs Macro Lett 2013, 2 (11), 1026–1032.
24. Su H; Li YW; Yue K; Wang Z; Lu PT; Feng XY; Dong XH; Zhang S; Cheng SZD; Zhang WB, Macromolecular structure evolution toward giant molecules of complex structure: tandem synthesis of asymmetric giant gemini surfactants. Polym Chem-Uk 2014, 5 (11), 3697–3706.
25. Tang W; Becker ML, “Click” reactions: a versatile toolbox for the synthesis of peptide-conjugates. Chem Soc Rev 2014, 43 (20), 7013–7039. [PubMed: 24993161]
26. Ning X; Guo J; Wolfert MA; Boons GJ, Visualizing metabolically labeled glycoconjugates of living cells by copper-free and fast huisgen cycloadditions. Angew Chem Int Ed Engl 2008, 47 (12), 2253–5. [PubMed: 18275058]
27. Chang PV; Prescher JA; Sletten EM; Baskin JM; Miller IA; Agard NJ; Lo A; Bertozzi CR, Copper-free click chemistry in living animals. Proc Natl Acad Sci U S A 2010, 107 (5), 1821–6. [PubMed: 20080615]
28. Liu X; Gong P; Song P; Xie F; Miller II AL; Chen S; Lu L, Rapid conjugation of nanoparticles, proteins and siRNAs to microbubbles by strain-promoted click chemistry for ultrasound imaging and drug delivery. Polym Chem-Uk 2019, 10 (6), 705–717.
29. Ono RJ; Lee AL; Voo ZX; Venkataraman S; Koh BW; Yang YY; Hedrick JL, Biodegradable strain-promoted click hydrogels for encapsulation of drug-loaded nanoparticles and sustained release of therapeutics. Biomacromolecules 2017, 18 (8), 2277–2285. [PubMed: 28682629]
30. Tyler DS; Vappiani J; Cañeque T; Lam EY; Ward A; Gilan O; Chan Y-C; Hienzsch A; Rutkowska A; Werner T, Click chemistry enables preclinical evaluation of targeted epigenetic therapies. Science 2017, eaal2066.

31. Liu X; Miller AL; Fundora KA; Yaszemski MJ; Lu L, Poly (ε-caprolactone) Dendrimer Cross-Linked via Metal-Free Click Chemistry: Injectable Hydrophobic Platform for Tissue Engineering. Acs Macro Lett 2016, 5, 1261–1265.
32. Zheng JK; Callahan LAS; Hao JK; Guo K; Wesdemiotis C; Weiss RA; Becker ML, Strain-Promoted Cross-Linking of PEG-Based Hydrogels via Copper-Free Cycloaddition. Acs Macro Lett 2012, 1 (8), 1071–1073. [PubMed: 23205321]
33. Xu JW; Filion TM; Prifti F; Song J, Cytocompatible Poly(ethylene glycol)-co-polycarbonate Hydrogels Cross-Linked by Copper-Free, Strain-Promoted Click Chemistry. Chem-Asian J 2011, 6 (10), 2730–2737. [PubMed: 21954076]
34. Shelbourne M; Chen X; Brown T; El-Sagheer AH, Fast copper-free click DNA ligation by the ring-strain promoted alkyne-azide cycloaddition reaction. Chem Commun 2011, 47 (22), 6257–6259.
35. Thibault RA; Scott Baggett L; Mikos AG; Kasper FK, Osteogenic differentiation of mesenchymal stem cells on pregenerated extracellular matrix scaffolds in the absence of osteogenic cell culture supplements. Tissue Engineering Part A 2009, 16 (2), 431–440.
36. Henry MG; Cai L; Liu XF; Zhang L; Dong JY; Chen L; Wang ZQ; Wang SF, Roles of Hydroxyapatite Allocation and Microgroove Dimension in Promoting Preosteoblastic Cell Functions on Photocured Polymer Nanocomposites through Nuclear Distribution and Alignment. Langmuir 2015, 31 (9), 2851–2860. [PubMed: 25710252]
37. Cai L; Foster CJ; Liu XF; Wang SF, Enhanced bone cell functions on poly(epsilon-caprolactone) triacrylate networks grafted with polyhedral oligomeric silsesquioxane nanocages. Polymer 2014, 55 (16), 3836–3845.
38. Wang SF; Yaszemski MJ; Knight AM; Gruetzmacher JA; Windebank AJ; Lu LC, Photo-crosslinked poly(epsilon-caprolactone fumarate) networks for guided peripheral nerve regeneration: Material properties and preliminary biological evaluations. Acta Biomater 2009, 5 (5), 1531–1542. [PubMed: 19171506]
39. Kutikov AB; Song J, Biodegradable PEG-based amphiphilic block copolymers for tissue engineering applications. Acs Biomater Sci Eng 2015, 1 (7), 463–480. [PubMed: 27175443]
40. Neumann AJ; Quinn T; Bryant SJ, Nondestructive evaluation of a new hydrolytically degradable and photo-clickable PEG hydrogel for cartilage tissue engineering. Acta Biomater 2016, 39, 1–11. [PubMed: 27180026]
41. Cao L; Cao B; Lu C; Wang G; Yu L; Ding J, An injectable hydrogel formed by in situ cross-linking of glycol chitosan and multi-benzaldehyde functionalized PEG analogues for cartilage tissue engineering. Journal of Materials Chemistry B 2015, 3 (7), 1268–1280. [PubMed: 32264478]
42. Kinard LA; Kasper FK; Mikos AG, Synthesis of oligo(poly(ethylene glycol) fumarate). Nat Protoc 2012, 7 (6), 1219–27. [PubMed: 22653160]
43. Lasprilla AJ; Martinez GA; Lunelli BH; Jardini AL; Maciel Filho R, Poly-lactic acid synthesis for application in biomedical devices—A review. Biotechnol Adv 2012, 30 (1), 321–328. [PubMed: 21756992]
44. Grayson ACR; Cima MJ; Langer R, Size and temperature effects on poly (lactic-co-glycolic acid) degradation and microreservoir device performance. Biomaterials 2005, 26 (14), 2137–2145. [PubMed: 15576189]
45. Kasper FK; Tanahashi K; Fisher JP; Mikos AG, Synthesis of poly (propylene fumarate). Nat Protoc 2009, 4 (4), 518–525. [PubMed: 19325548]
46. Dadsetan M; Guda T; Runge MB; Mijares D; LeGeros RZ; LeGeros JP; Silliman DT; Lu LC; Wenke JC; Baer PRB; Yaszemski MJ, Effect of calcium phosphate coating and rhBMP-2 on bone regeneration in rabbit calvaria using poly(propylene fumarate) scaffolds. Acta Biomater 2015, 18, 9–20. [PubMed: 25575855]
47. Fisher JP; Holland TA; Dean D; Engel PS; Mikos AG, Synthesis and properties of photocross-linked poly(propylene fumarate) scaffolds. Journal of Biomaterials Science, Polymer Edition 2001, 12 (6), 673–687. [PubMed: 11556743]
48. Olthof MGL; Kempen DHR; Herrick JL; Yaszemski MJ; Dhert WJA; Lu L, Effect of different sustained bone morphogenetic protein-2 release kinetics on bone formation in poly(propylene

fumarate) scaffolds. Journal of Biomedical Materials Research Part B: Applied Biomaterials 2018, 106 (2), 477–487. [PubMed: 28186684]

49. Wang SF; Kempen DHR; de Ruiter GCW; Cai L; Spinner RJ; Windebank AJ; Yaszemski MJ; Lu LC, Molecularly Engineered Biodegradable Polymer Networks with a Wide Range of Stiffness for Bone and Peripheral Nerve Regeneration. Advanced Functional Materials 2015, 25 (18), 2715–2724.
50. Shi K; Wang Y-L; Qu Y; Liao J-F; Chu B-Y; Zhang H-P; Luo F; Qian Z-Y, Synthesis, characterization, and application of reversible PDLLA-PEG-PDLLA copolymer thermogels in vitro and in vivo. Sci Rep-Uk 2016, 6, 19077.
51. Asai D; Xu D; Liu W; Quiroz FG; Callahan DJ; Zalutsky MR; Craig SL; Chilkoti A, Protein polymer hydrogels by in situ, rapid and reversible self-gelation. Biomaterials 2012, 33 (21), 5451–5458. [PubMed: 22538198]
52. Ur-Rehman T; Tavelin S; Gröbner G, Chitosan in situ gelation for improved drug loading and retention in poloxamer 407 gels. Int J Pharmaceut 2011, 409 (1–2), 19–29.
53. Chaibundit C; Ricardo NM; Ricardo NM; Muryn CA; Madec M-B; Yeates SG; Booth C, Effect of ethanol on the gelation of aqueous solutions of Pluronic F127. Journal of colloid and interface science 2010, 351 (1), 190–196. [PubMed: 20708740]
54. Chiu R; Ma T; Smith RL; Goodman SB, Polymethylmethacrylate particles inhibit osteoblastic differentiation of MC3T3-E1 osteoprogenitor cells. J Orthop Res 2008, 26 (7), 932–936. [PubMed: 18302244]
55. Frydrych M; Román S; MacNeil S; Chen B, Biomimetic poly (glycerol sebacate)/poly (l-lactic acid) blend scaffolds for adipose tissue engineering. Acta Biomater 2015, 18, 40–49. [PubMed: 25769230]
56. Roman S; Mangera A; Osman NI; Bullock AJ; Chapple CR; MacNeil S, Developing a tissue engineered repair material for treatment of stress urinary incontinence and pelvic organ prolapse—which cell source? Neurourology and urodynamics 2014, 33 (5), 531–537. [PubMed: 23868812]
57. Oftadeh R; Perez-Viloria M; Villa-Camacho JC; Vaziri A; Nazarian A, Biomechanics and mechanobiology of trabecular bone: a review. Journal of biomechanical engineering 2015, 137 (1), 010802.
58. Keaveny TM; Morgan EF; Yeh OC, Bone mechanics. Standard handbook of biomedical engineering and design 2004, 1–24.
59. Liu X; Paulsen A; Giambini H; Guo J; Miller AL; Lin P-C; Yaszemski MJ; Lu L, A New Vertebral Body Replacement Strategy Using Expandable Polymeric Cages. Tissue Engineering Part A 2016, 23 (5–6), 223–232. [PubMed: 27835935]
60. Teng Y; Giambini H; Rezaei A; Liu X; Miller AL; Waletzki BE; Lu L, Poly (Propylene Fumarate)–Hydroxyapatite Nanocomposite Can Be a Suitable Candidate for Cervical Cages. Journal of Biomechanical Engineering 2018, 140 (10), 101009.
61. Woodruff MA; Hutmacher DW, The return of a forgotten polymer-Polycaprolactone in the 21st century. Prog Polym Sci 2010, 35 (10), 1217–1256.
62. Xu LC; Siedlecki CA, Effects of surface wettability and contact time on protein adhesion to biomaterial surfaces. Biomaterials 2007, 28 (22), 3273–83. [PubMed: 17466368]
63. Leggat PA; Smith DR; Kedjarune U, Surgical applications of methyl methacrylate: a review of toxicity. Archives of environmental & occupational health 2009, 64 (3), 207–212. [PubMed: 19864224]
64. Dormer W; Gomes R; Meek M, Methyl methacrylate. World Health Organization 1998.
65. Methylene chloride. World Health Organization 1984.
66. Methyl Methacrylate, Centers for Disease Control and Prevention (CDC). https://www.cdc.gov/niosh/idlh/80626.html.
67. Methylene Chloride, Centers for Disease Control and Prevention (CDC). https://www.cdc.gov/niosh/idlh/75092.html.
68. Kimura ET; Ebert DM; Dodge PW, Acute toxicity and limits of solvent residue for sixteen organic solvents. Toxicology and applied pharmacology 1971, 19 (4), 699–704. [PubMed: 5132037]
69. Gao C; Peng S; Feng P; Shuai C, Bone biomaterials and interactions with stem cells. Bone research 2017, 5, 17059. [PubMed: 29285402]

70. Alizadeh-Osgouei M; Li Y; Wen C, A comprehensive review of biodegradable synthetic polymer-ceramic composites and their manufacture for biomedical applications. Bioactive materials 2019, 4 (1), 22–36. [PubMed: 30533554]

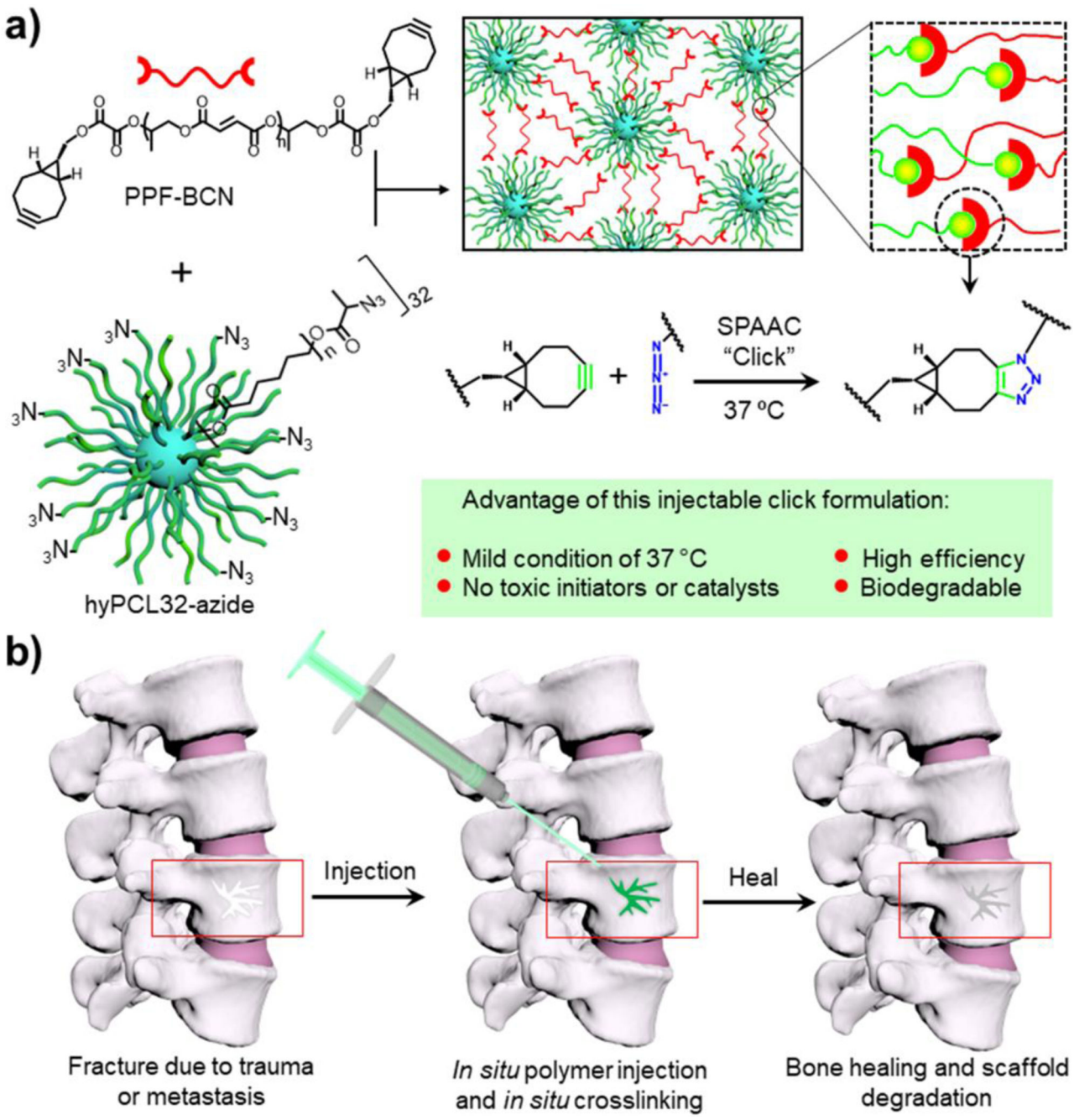

Figure 1.

Schematic demonstration of the polymer crosslinking mechanism and potential applications. a) Injectable system composted of PPF-BCN and hyPCL32-N_3 that can be self-crosslinked by SPAAC click chemistry after mixing. b) Schematic demonstration of potential applications of the injectable formulation for spine defect filling in bone tissue engineering.

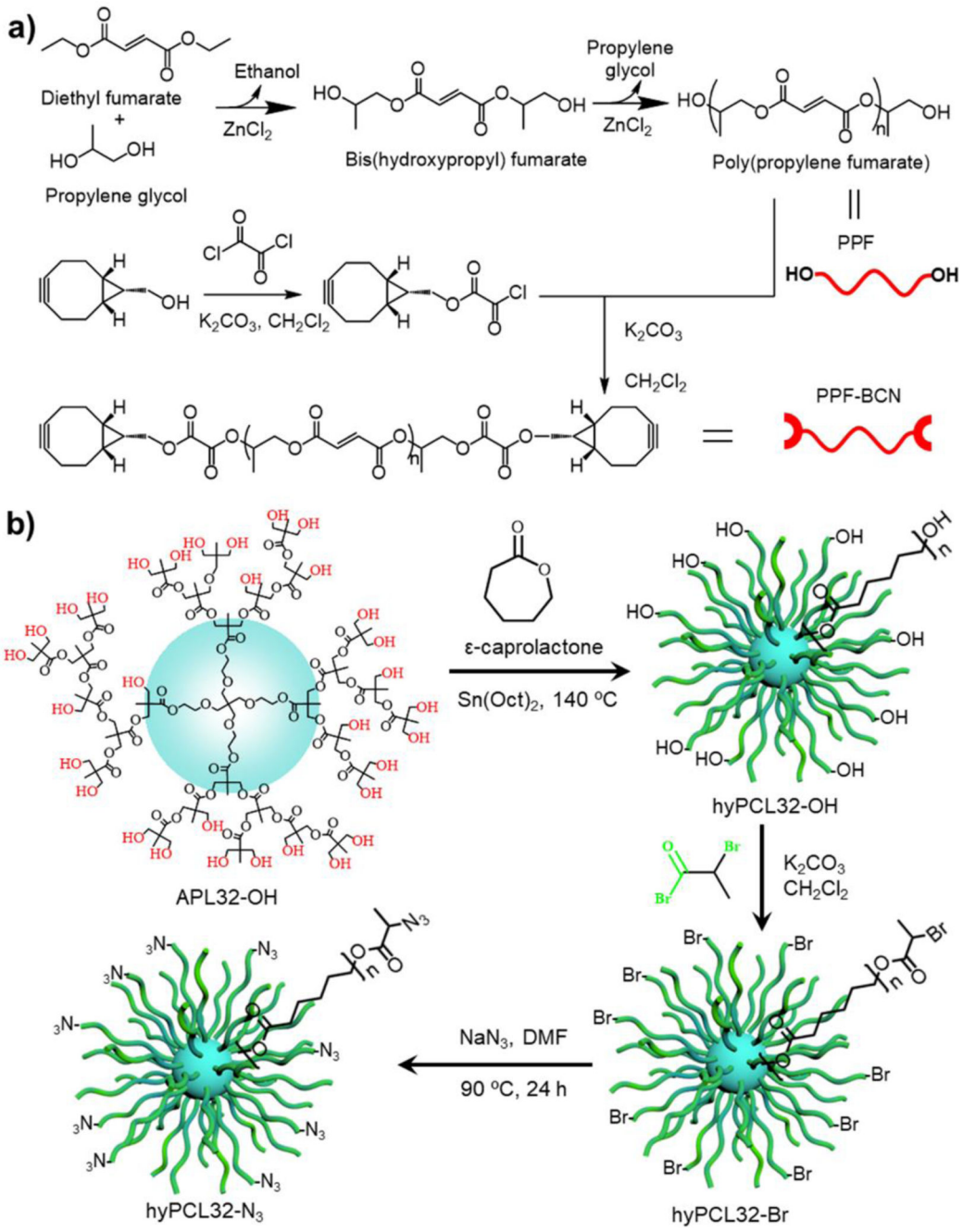

Figure 2.

Synthetic schemes of polymers. a) Synthesis of PPF-BCN polymer using diethyl fumarate, propylene glycol, and BCN-OH. B) Synthesis of hyPCL32-N_3 dendrimer by ring-opening reaction of ε-caprolactone using a hyperbranched 32-arm dendrimer bis-MPA polyester-32-hydroxyl (APL32-OH) core, followed by the addition of azide group using sodium azide.

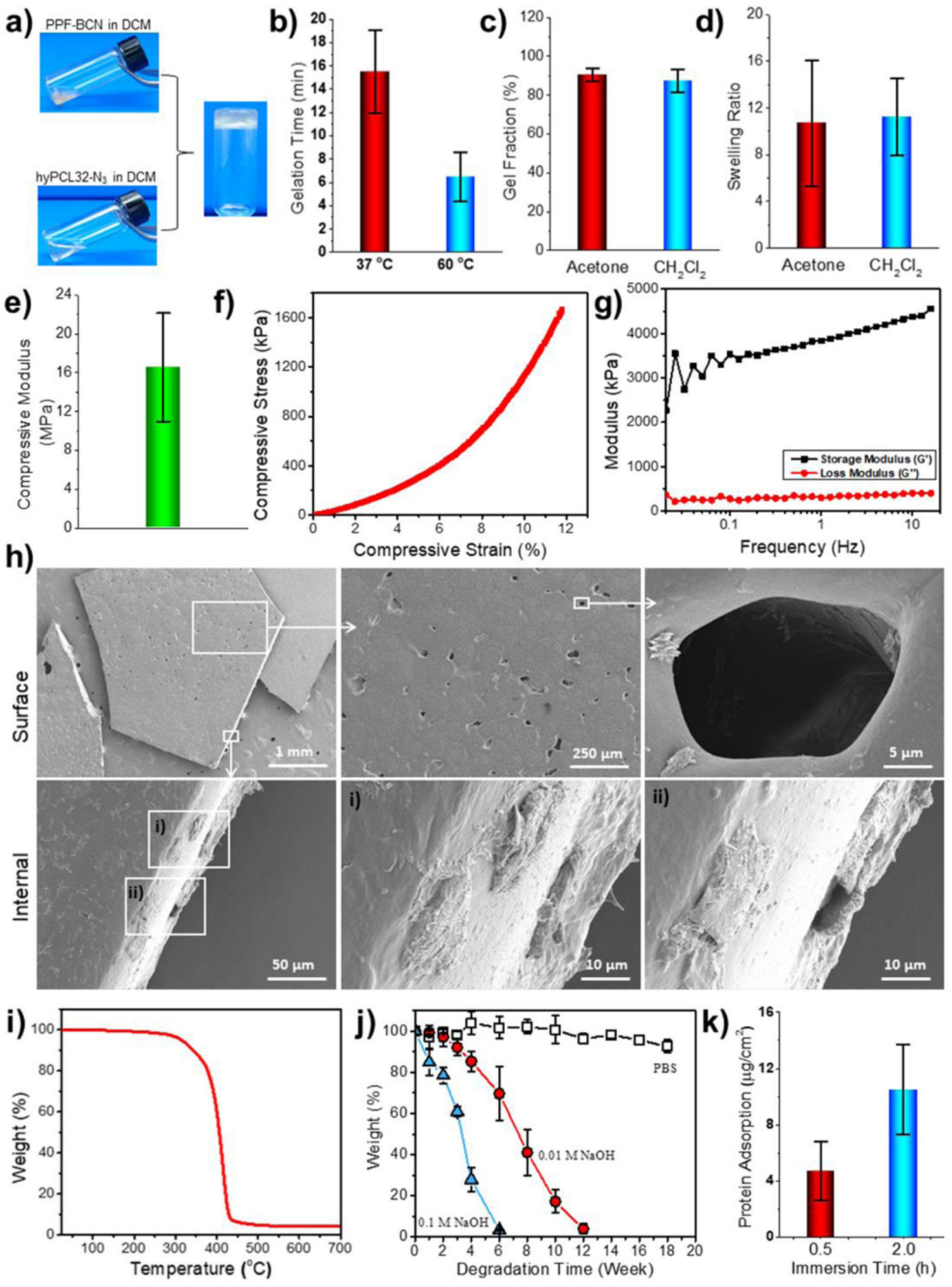

Figure 3.

Characterization of crosslinked PFCL-Click scaffolds. a) Photographs of PPF-BCN and hyPCL32-N_3 dissolved in dichloromethane (CH_2Cl_2) and gelled specimen after mixing. b). Gelation time at temperatures of 37 °C and 60 °C. c) Gel fraction and d) swelling ratio of crosslinked PFCL-Click scaffold in acetone or CH_2Cl_2. Mechanical properties including e) compressive moduli, f) compressive strain-stress curve, and g) frequency sweep test of the crosslinked PFCL-Click scaffold. h) SEM images showing the surface and internal morphologies of crosslinked PFCL-Click scaffolds. i) Thermal degradation of crosslinked PFCL-Click scaffold during thermogravimetric analysis from room temperature to 700 °C. j)

Degradation of crosslinked PFCL-Click scaffold in 0.1 M NaOH, 0.01 M NaOH, and PBS. k) Protein adsorption at 0.5 and 2 hours after immersion into the cell culture medium.

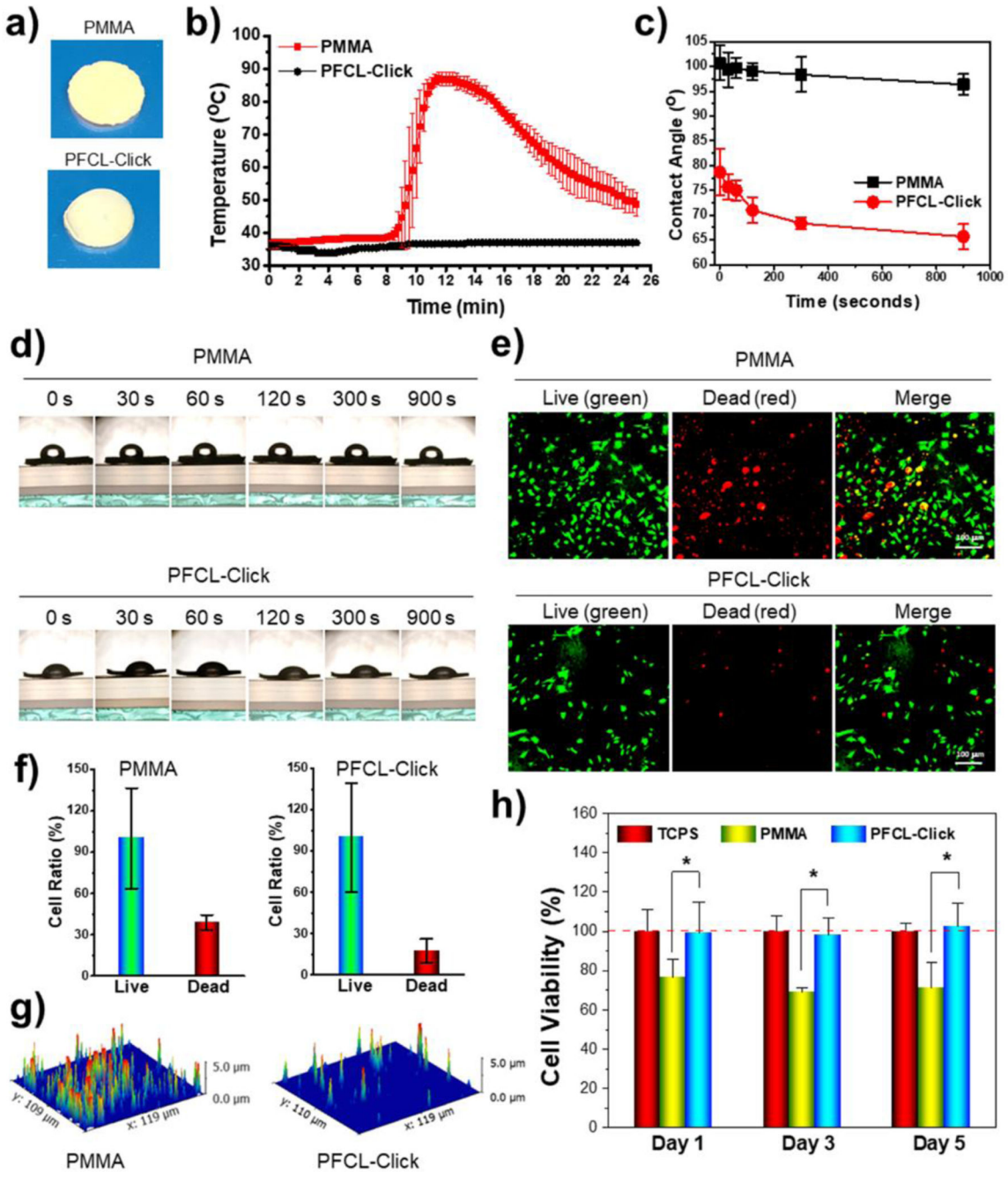

Figure 4.

Temperature change during crosslinking and wettability and cytotoxicity of crosslinked PFCL-Click scaffolds. a) Photographs of crosslinked PFCL-Click and control PMMA specimens. b) Temperature change during the crosslinking process for PFCL-Click scaffold and PMMA control. c) Water contact angle and d) photographs of water droplets on crosslinked PFCL-Click scaffold demonstrating hydrophobic surfaces. e) Live/dead staining of MC3T3 pre-osteoblast cells on the crosslinked PFCL-Click scaffold and PMMA control after 1 day of culture. f) Quantitative analysis of relative live cell and dead cell ratios from the live/dead images (set live cells number as 100%). g) 3D reconstruction of dead

cell fluorescence signal map. h) MTS analysis of cytotoxicity of PFCL-Click scaffold and PMMA control to MC3T3 cells. *: Statistically different ($p < 0.05$).

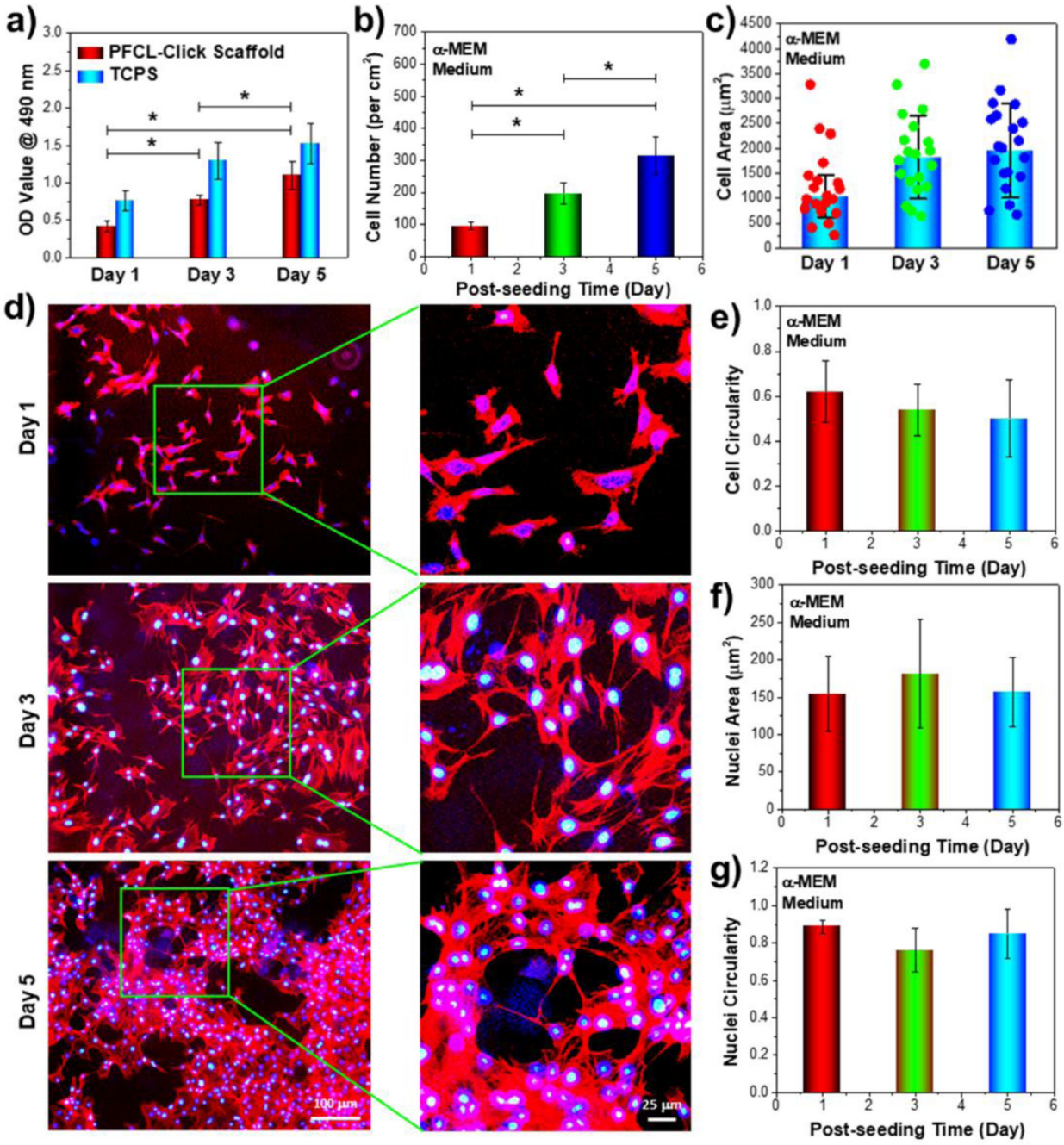

Figure 5.

Pre-osteoblast cell growth on the crosslinked PFCL-Click scaffold. a) MC3T3 cell proliferation on the crosslinked PFCL-Click scaffolds determined by MTS assay at 1, 3, and 5 days post-seeding. b) Cell numbers and c) cell areas calculated from d) immune-fluorescence images of the cells growing on the crosslinked PFCL-Click scaffolds (red: F-actin stained with rhodamine-phalloidin; blue: cell nuclei stained with DAPI). e) Cell circularity, f) nuclei area, and g) nuclei circularity of MC3T3 cells cultured on the crosslinked PFCL-Click scaffolds at 1, 3, and 5 days post-seeding. *: Statistically different ($p < 0.05$).

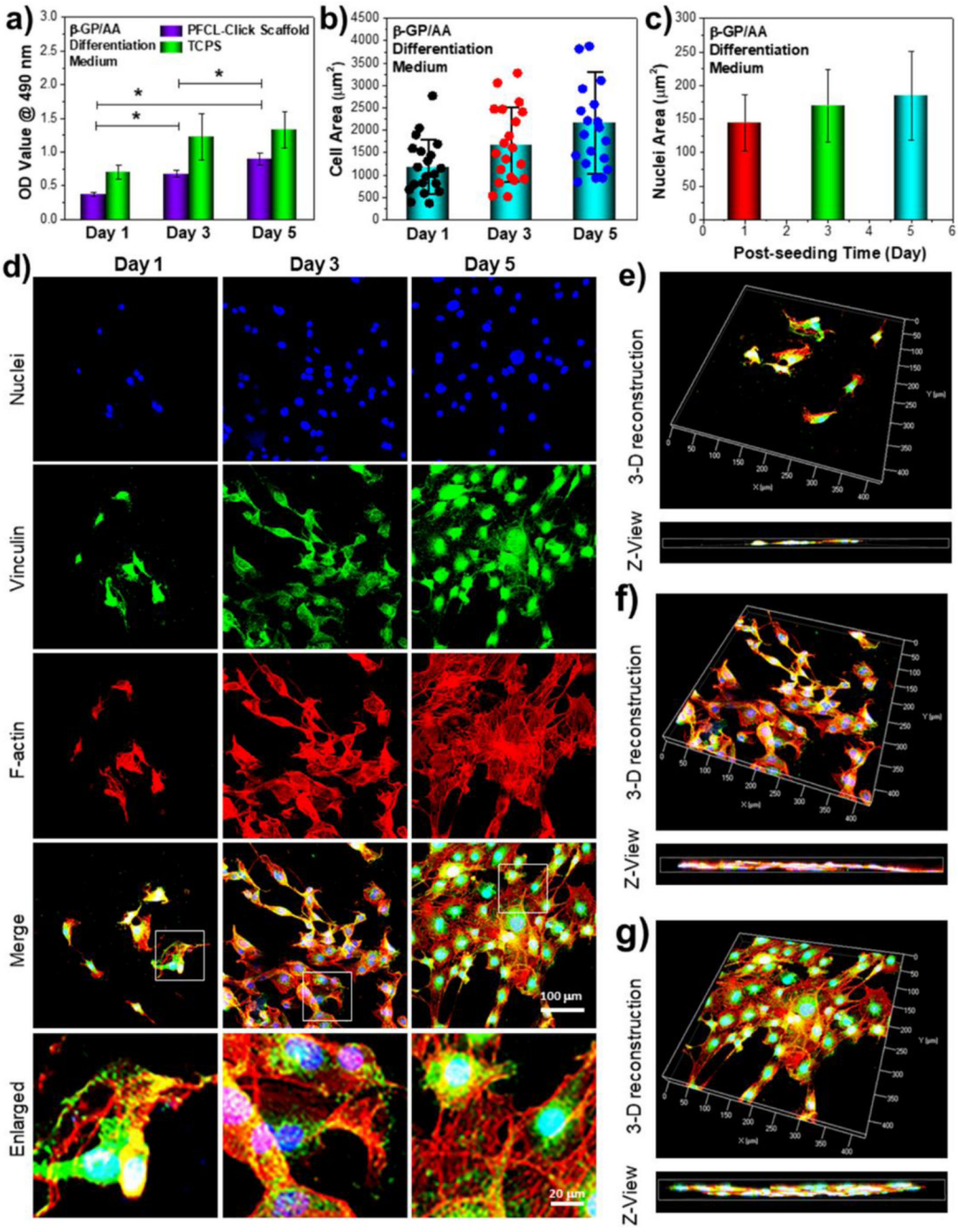

Figure 6.

Pre-osteoblast cell behavior under differentiation medium induction on the crosslinked PFCL-Click scaffold. The a) cell numbers and b) cell area and c) nuclei area of the MC3T3 cells in differentiation medium at 1, 3, and 5 days post-seeding on crosslinked PFCL-Click scaffolds. d) Immune-fluorescence images of MC3T3 cells cultured on crosslinked PFCL-Click scaffolds in osteogenic medium supplemented with 10 mM β-glycerophosphate (β-GP) and 50 μg/mL ascorbic acid (AA). The 3-D reconstruction of MC3T3 cells in the differentiation medium at e) 1 day, f) 3 day and g) 5 days post-seeding on crosslinked PFCL-Click scaffolds. *: Statistically different ($p < 0.05$).

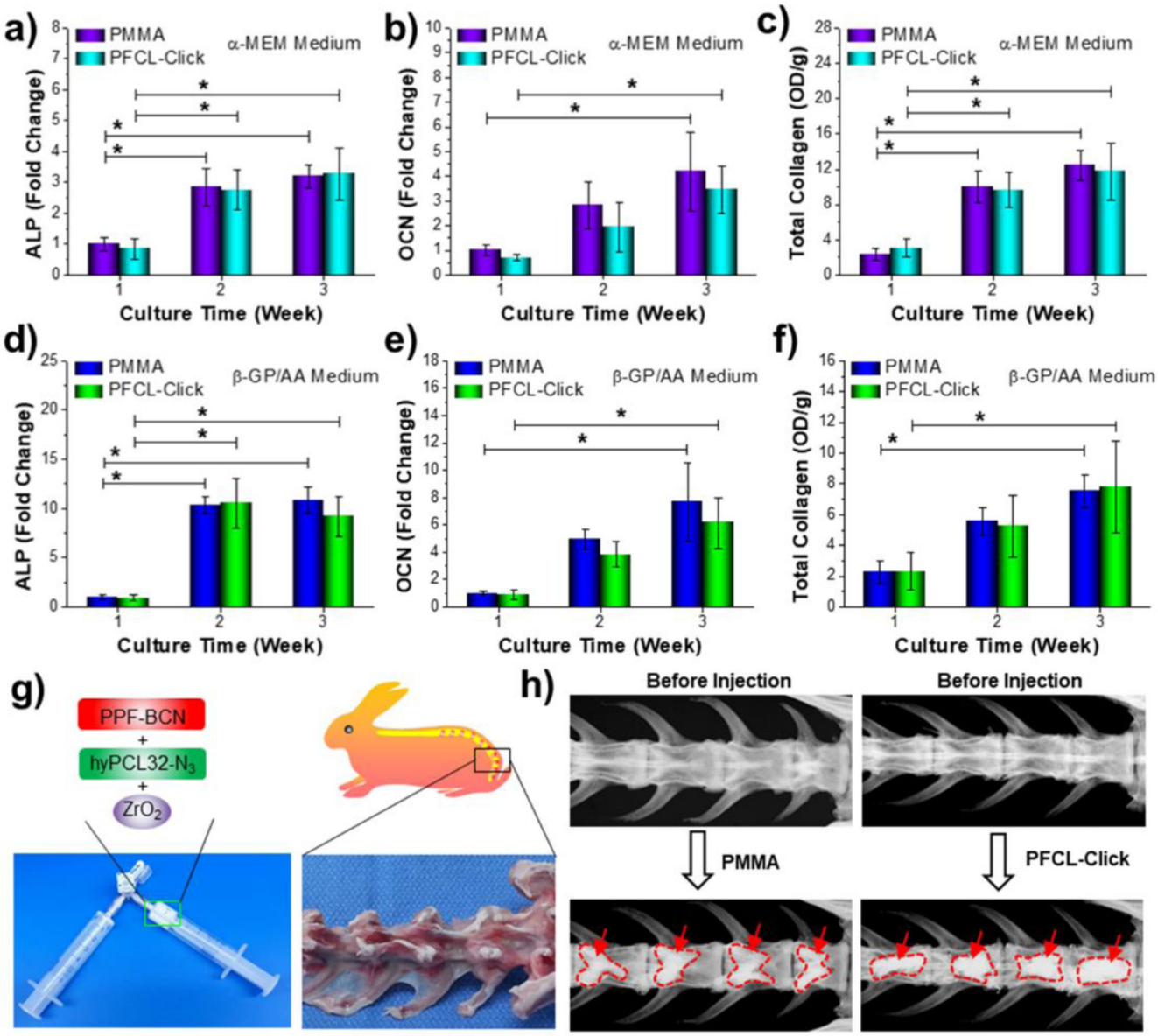

Figure 7.

Osteogenesis of pre-osteoblast cell and rabbit spine injection. a) Intracellular ALP, b) OCN and c) total collagen production of MC3T3 pre-osteoblast cells cultured on crosslinked PFCL-Click scaffolds with α-MEM medium for 1, 2, and 3 weeks. After culture in an osteogenic medium supplemented with 10 mM β-glycerophosphate and 50 μg/mL ascorbic acid for 1, 2, 3 weeks, the d) intracellular ALP, e) OCN and f) total collagen production of MC3T3 pre-osteoblast cells were also determined. g) Photographs of PPF-BCN mixed with hyPCL32-N_3 and incorporated with ZrO_2. h) X-ray images of the PFCL-Click/ZrO_2 system after injection to the rabbit vertebral bodies. *: Statistically different ($p < 0.05$).